Materials Chemistry and Physics 295 (2023) 127046

Contents lists available at ScienceDirect

Materials Chemistry and Physics

journal homepage: www.elsevier.com/locate/matchemphys

Production of bovine hydroxyapatite nanoparticles as a promising biomaterial via mechanochemical and sonochemical methods

Brunna Mota Ferrairo [a], Victor Mosquim [b], Lucas José de Azevedo-Silva [a], Luara Aline Pires [b], David Santos Souza Padovini [c], Aroldo Geraldo Magdalena [c], Carlos Alberto Fortulan [d], Paulo Noronha Lisboa-Filho [e], José Henrique Rubo [a], Ana Flávia Sanches Borges [b,*]

[a] Department of Prosthodontics and Periodontics, Bauru School of Dentistry, University of São Paulo. Alameda Dr. Octávio Pinheiro Brisolla, 9-75, Vila Universitária, ZIP CODE: 17012-901. Bauru, São Paulo, Brazil
[b] Department of Operative Dentistry, Endodontics and Dental Materials, Bauru School of Dentistry, University of São Paulo. Alameda Dr. Octávio Pinheiro Brisolla, 9-75, Vila Universitária, ZIP CODE: 17012-901. Bauru, São Paulo, Brazil
[c] Department of Chemistry, School of Sciences, São Paulo State University. Eng. Luís Edmundo Carrijo Coube, 2085 - Nucleo Res. Pres. Geisel, ZIP CODE: 17033-360. Bauru, São Paulo, Brazil
[d] Department of Mechanical Engineering, São Carlos School of Engineering, University of São Paulo. Av. Trab. São Carlense, 400 - Parque Arnold Schimidt, ZIP CODE: 13566-590. São Carlos, São Paulo, Brazil
[e] Department of Physics, School of Sciences, São Paulo State University. Av. Eng. Luís Edmundo Carrijo Coube, 2085 - Nucleo Res. Pres. Geisel, ZIP CODE: 17033-360. Bauru, São Paulo, Brazil

HIGHLIGHTS

- Sonochemical and milling techniques were able to nanoparticle bovine hydroxyapatite preserving the crystal structure.
- The average grain size was 40 nm for the milling technique and 60 nm for the sonication.
- This material represents a promising bioactive material for future use in dentistry.

GRAPHICAL ABSTRACT

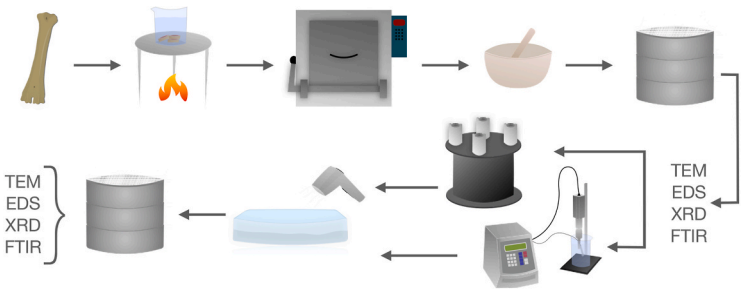

ARTICLE INFO

Keywords:
Ceramic material
Nanoparticles
Nanostructured materials
Hydroxyapatite

ABSTRACT

This study aimed to evaluate the effectiveness of sonochemical and milling nanoparticulate techniques using HA of bovine origin. The starting powders were characterized using X-ray diffraction (XRD), Fourier transform infrared (FTIR) spectroscopy, scanning electron microscopy (SEM), energy-dispersive spectroscopy (EDX), and transmission electron microscopy (TEM) (75 μm). Sonication was performed with 40% of the maximum amplitude (750 W) and 20 Hz in an aqueous solution (4 h). The milling technique used a polyethylene jug loaded with 40 vol% milling elements placed in a rotatory mill (104 rpm, 48 h), then in a vibratory mill (72 h). The results revealed that the final average grain size of HA was 40 nm for the milling technique and 60 nm for the sonication (TEM). FTIR analysis showed a broad band at 1300–500 cm−1, and similar peaks without HA bond degradation, regardless of the two forms of HA nanoparticles. XRD analysis showed peaks equivalent to those of

* Corresponding author.
E-mail address: afborges@fob.usp.br (A.F. Sanches Borges).

https://doi.org/10.1016/j.matchemphys.2022.127046
Received 17 June 2022; Received in revised form 9 November 2022; Accepted 14 November 2022
Available online 16 November 2022

synthetic and animal HA. In addition, the equivalence between the method peaks demonstrated non-degradation of structural. The same chemical characteristics between groups were also observed in the EDX samples. We concluded that both methods were able to decrease the size of particles preserving the crystal structure, but the milling method produced smaller particles.

1. Introduction

Hydroxyapatite ($Ca_{10}(PO_4)_6(OH)_2$, (HA) is widely used for skeletal and dental reconstructions because of its excellence in properties such as biocompatibility, bioactivity, high osteoconduction and/or osteoinduction, nontoxicity, noninflammatory behavior, and non-immunogenicity [1–3]. The search for alternative sources is influenced by the limited supply of autologous bone and its high applicability and consumption.

The extraction of HA from biological resources, such as biogenic (eggshells, seashells, and calcite materials), plant (bamboo, calendula flower, etc.), and bone (mammalian and fish bones) sources, from sanitary, economic, and environmental points of view, is a safer and more balanced option for obtaining biomaterials [4,5]. Moreover, the organic components and possible pathogens are eliminated during the calcination process, leaving only the mineral component with beneficial trace ions that speed up the bone-formation process [6].

The nanoscale form of HA can significantly increase the biocompatibility and bioactivity of HA [7] as it presents a high ratio between surface area and volume, approaching the size and chemical composition of the human bone tissue [8]. Manipulating this material at the atomic and molecular levels improves the mechanical stability of the bone frame and provides a more appropriate chemical surface and porosity for cell proliferation, optimizing biocompatibility [9–11].

There are several methods described for HA nanoparticulation. The main synthesis techniques can be grouped into 1) dry methods; 2) wet methods; 3) processes at high temperatures; 4) synthesis methods based on biogenic sources, and; 5) a combination of these [5]. In this study, two nanoparticulation methods were selected. An initial thermal step of calcination was equivalent for both groups and after a representative of the dry methods (mechanochemical method) and one of the wet methods (sonochemical method) were selected. Both are classified as low cost and could obtain nanometric particles with diverse morphologies and different degrees of crystallinity, degrees of purity, and Ca/P ratios [5].

It is of great interest not only to evaluate the particle size reduction capacity of the methods from biological resources, but also the quality of their physical and chemical properties, which are crucial aspects to achieve optimal properties. This study aimed to achieve bovine HA particles at nanoscale and to evaluate the effect two methods on the nanoparticles by inspection of physical and chemical characteristics. The study null hypothesis was that the nanoparticles produced by the two methods would show similar physical and chemical characteristics by X-ray diffraction (XRD) associated with Rietveld refinements, Fourier transform infrared spectroscopy (FT-IR), energy dispersive X-ray spectroscopy (EDX), and transmission electron microscopy (TEM).

2. Materials and methods

2.1. Obtainment of HA

The extraction of HA from bovine bones is intended to be sustainable: recovering and processing residues that would be discarded in landfills or used to produce animal food. In this study, the organic matter in bovine femurs was removed via a thermochemical process [12], and the remaining material from the femurs was reduced using mortars and pestles. The samples were subjected to chemical and cytotoxic analyses to verify the absence of heavy metals and biological contamination in the bone composition. Once the results for these components were negative, the bones were released for further use.

To obtain a uniform and submicrometric powder, the granules were milled in a jug of polyethylene (85 mm of height and 300 cm^3 of volume) and loaded with 40% vol (500 g) of spheres of 3Y zirconia ∅ 3 mm, para-aminobenzoic acid ($C_7H_7NO_2$) as deflocculant and isopropyl alcohol (C_3H_8O) as the solvent of the liquid medium binder solvent. The jar was filled with a concentration of 30 vol% solids and placed in a gyratory mill (104 rpm for 48 h), then a vibratory mill (72 h). The samples were dried in an oven at 80 °C and granulated in stainless steel sieves of #200 mesh ≤75 μm.

2.2. Initial characterization

XRD patterns characterize the structural phase (Rigaku D/MAX 2500 PC with CuKα radiation source (λ = 1.54056 Å) with rotatory anode operation at 40 KV and 150 mA). The Scherrer equation[26] was used to determine the crystallite size of the HA:

$$D = \frac{0.9\lambda}{\mathrm{FWHM} \bullet cos\ \theta} \quad (1)$$

where the crystallite size (nm), the wavelength is λ (0.0154056 nm), the full width at half maximum (FWHM) of the diffraction peak under consideration (rad) and the diffraction angle θ (deg). PANalytical X'Pert HighScore and PCPDFWIN software were used to propose standards and evaluate the XRD profiles according to the International Centre for Diffraction Data (ICDD).

The FT-IR spectra were recorded (FTIR-Vertex 70, Bruker) with KBr in the transmittance mode in the range of 500–2500 cm^{-1} to investigate the functional groups of the resultant powders.

For semi-quantitative examination, EDX was coupled with scanning electron microscopy (SEM, SERON AIS-2100). The samples were coated with gold at a thickness of 10 nm and were investigated using an XL30 FEG, an ultra-vacuum system with a base pressure of 1×10^{-5} Pa and an acceleration voltage of 20 kV.

For further structural analysis that aimed to explore individual nanostructures and measure the initial particle size and agglomeration phenomenon, TEM (Philips CM200) was performed at 200 kV. Samples were prepared by dropping a diluted suspension over a 300-mesh carbon-coated copper grid and drying the excess solution with semi-permeable paper. Images were obtained to identify the crystallographic orientations and crystallinity of the nanoparticles.

X-ray fluorescence analysis by wavelength dispersion (WDXRF) was also performed to verify whether the chemical composition was in accordance with ASTM F1185-03, which determines the maximum concentration of heavy metals allowed for HA of animal origin.

2.3. Methods of nanoparticulation

To test the efficiency of the particle, decrease without degradation, two methods were selected.

2.3.1. Ball mill

Using a polyethylene jug (300 cm^3) loaded with 40 vol% (500 g) milling elements (3Y zirconia balls, HA, isopropyl alcohol, and para-aminobenzoic acid) placed in a ball mill (104 rpm, 48 h) and then in a vibratory mill (72 h), grinding was performed. After that, the alcohol was evaporated with the aid of a heated air blower (≅ 80 °C) and the powder was granulated in stainless steel sieves of # 200 mesh ≤75 μm.

2.3.2. Sonochemical

HA powder was subjected to ultrasonic processing in a Sonics brand model VCX-750 Vibra-Cell Ultrasonic Liquid Processor using 750 W of power and a frequency of 20 kHz for 4 h with pulses of 5 min in duration and variable amplitude fixed at up to 40% from the nominal amplitude of the equipment (750 W/cm^2). The Ca/P molar ratio was fixed at 1.67, and the concentration of the Ca^{2+} ions was 0.02. The aqueous solution (deionized water–Milli-Q® systems) was chosen for its purity to avoid contamination and chemical interaction during acoustic cavitation. Although its high vapor pressure (17.5 mmHg, 0 Â °C), the samples were cooled in an ice bath, and deionized water was added to maintain the solution at a constant volume and standardize the effect of acoustic cavitation.

To prevent particle agglomeration, ammonium polyacrylate deflocculant ($C_3H_4O_2$, NHPA) was added to the mixture during sonication (0.1 wt.%) [13]. After the sonication, the aqueous portion was dried in an oven at 80 °C and granulated in stainless steel sieves of #200 mesh ≤75 μm.

2.4. Final characterization

After performing the nanoparticulation methods, samples in liquid medium were submitted to TEM, and dry samples were collected for XRD, FTIR and EDX.

The methodological design of this study was summarized by Fig. 1.

3. Results and discussion

Decreasing the particle size with the maintenance of an appropriate stoichiometry, morphology, and purity is fundamental [14].

There are methods capable of controlling the geometry, size distribution, crystallographic, and chemical structure which reflects in great mechanical, in vitro, and in vivo biological properties [5]. Combined methods have been frequently used, and these methods seem to improve the final properties of HA that is derived from natural sources [5]. For bovine bones, the most frequent association of nanoparticulation methods is hydrothermal and calcination [15]. The present study demonstrates that the association between calcination and sonochemical or ball milling also provides promising results of reaction kinetics, reduction of particle size, and high purity.

The FTIR spectra of the samples and the amplification of bands at 1300–1500 cm^{-1} are presented in Fig. 2. A narrow band near 965 cm^{-1} represents the v1 mode of PO_4^{3-} ions apatite present in all spectra of HA and carbonated apatite. The band at 469 cm^{-1} is assigned to the v2 phosphate mode in the bending vibration, and it does not appear in the spectrum. The v2 band of CO_3^{2-} is located at range from 873 to 880 cm^{-1} (out-of-plane bending vibration), which results from out-of-plane stretching. The main signal of the phosphate group appears in the triply degenerate v3 domain (1100–1035 cm^{-1}). The v3 mode, between 1400 and 1600 cm^{-1}, is composed of two bands [16] and represents the strongest IR band for carbonate. The band at 700 cm^{-1} indicates C–O absorption, and its combination with the v3 signal indicates that no calcite was associated with HA [17]. The v4 phosphate mode appears at different sites for carbonated apatite (bending vibration): the 633, 603, and 565 cm^{-1} bands [18,19]. Frequently, carbonate ions are associated with impurities, that is, residual organic components, after calcination [20]. Absorbed water (1635 cm^{-1}) was almost imperceptible in the spectra. The slight presence of the characteristic peak at 650 cm^{-1} (shift to 660 cm^{-1}) due to v1(OH) in the HA could be better visualized using high-energy transfer inelastic neutron scattering spectroscopy [21]. As important as the identification of the peaks presented is the relevant observation of their maintenance of shapes and intensities of the absorption band in FT-IR spectra after performing the methods demonstrated, which demonstrates the preservation capacity of the methods.

Regarding nanoparticulation methods, both showed be friendly-performance. The bovine bone powder had white color, with some light-yellow parts, which shows the beginning of the organic matrix removal after the thermochemical process with 30% hydrogen peroxide (H_2O_2) as a 100-vol aqueous solution was heated to 100 °C. Previous literature has reported a successful pre-treatment that involves removing fat, protein, and soft tissues and cutting the bone into small pieces before boiling [22–24]. This process ensures that a larger surface area meets the chemical agents, providing a good sample. This pre-treatment was completed after calcination with a heating curve of

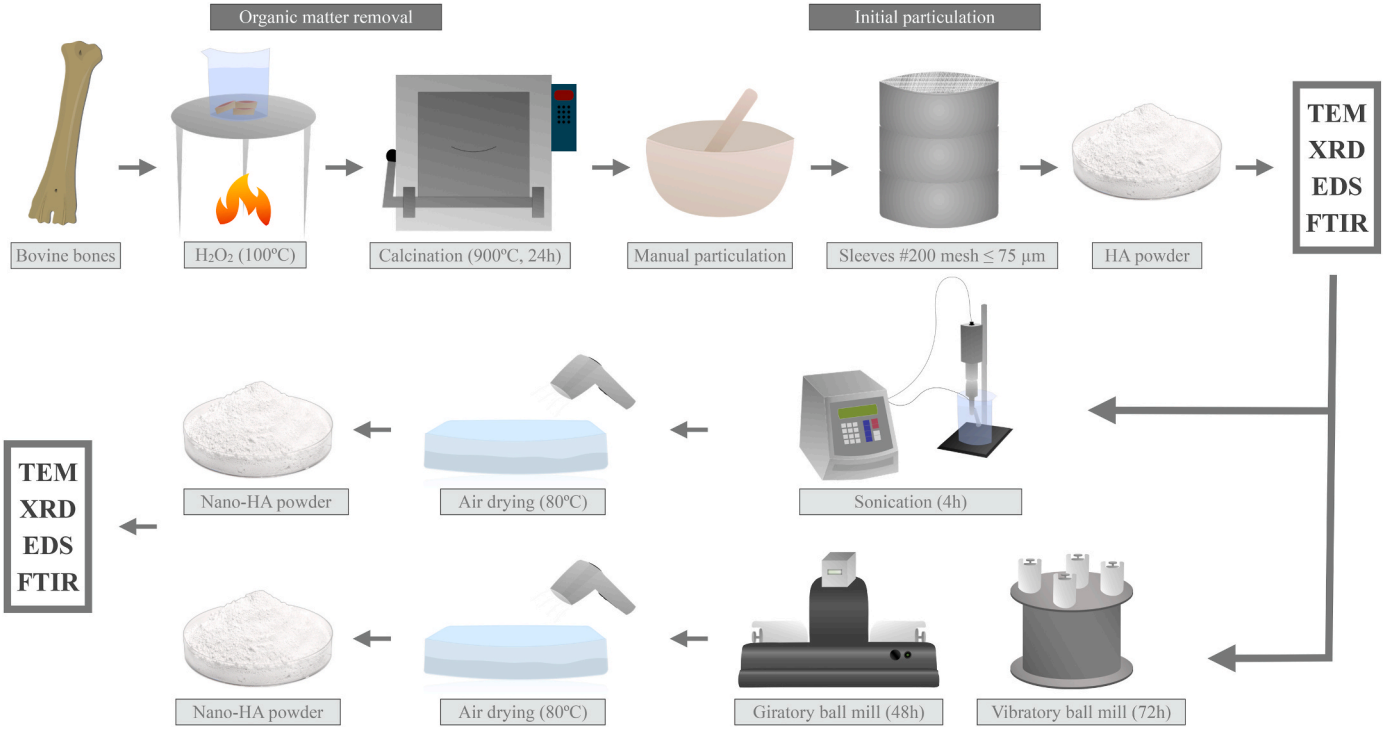

Fig. 1. Methodological flowchart.

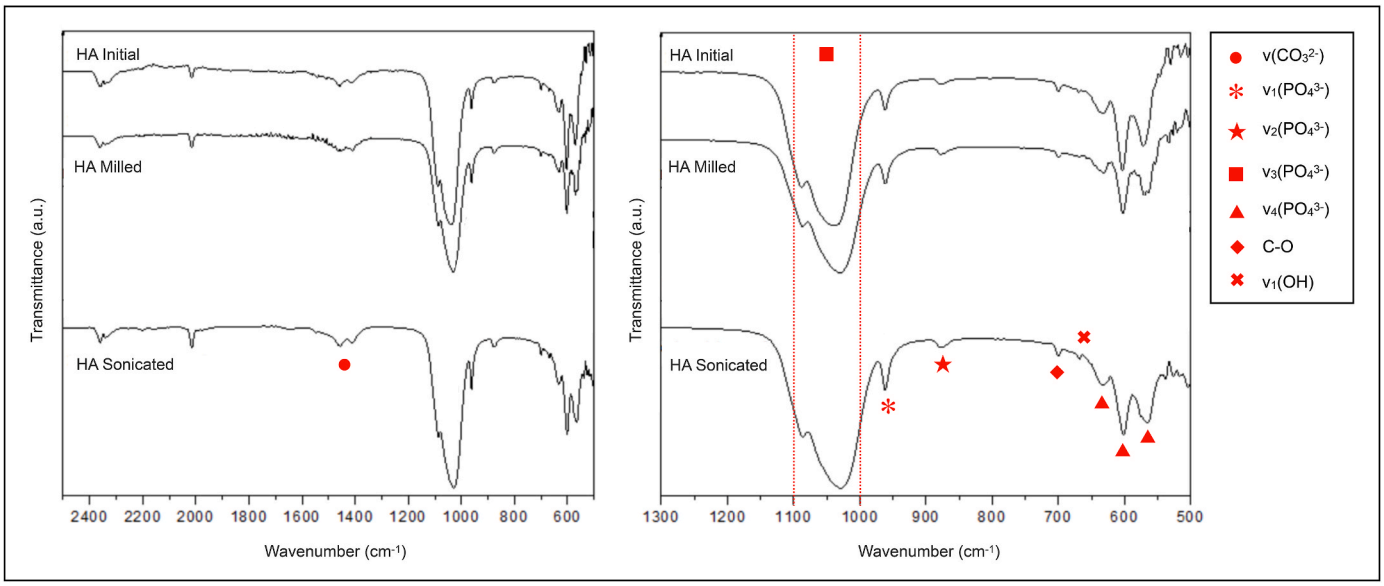

Fig. 2. FT-IR spectrum and the amplification of bands 1300–1500 cm-1 of HA precursor and after the nanoparticulation methods.

5 °C/min up to 900 °C, a 2-h plateau [25], and a long cooling time, which homogenized into a white color, with protein and collagen absence [26,27]. The use of the thermal method increases the crystallinity of particles [4], and the proper temperature for sintering HA from bovine bone is approximately 1000 °C based on two-thirds of its melting point [27]. A high temperature results in the degradation of the calcium phosphate, and β-tricalcium phosphate (β-TCP) starts to be obtained at 850 °C, and at 900 and 1000 °C, pure crystalline HA still can be produced [4]. The choice of 900 °C sintering temperature ensures that partial dehydration will initiate, as well as the production of β-TCP and a creeping reaction of hydroxides or carbonates to the respective oxides. This avoid the melting point of bovine bone, as demonstrated by studies with differential thermal analysis (DTA) [27–29]. Also, temperatures above 800 °C can eliminate all pathogens, preventing the possibility of disease transmission [30].

XRD is a relevant technique for identifying phases before and after nanoparticulation methods. Fig. 3 shows the XRD patterns, which demonstrate that the data are in accordance with previously reported descriptions of the XRD structure and characteristic patterns of bovine origin HA (XRD, JCPDS file no. 9–432, 1996) [31] and of the pure HA phase [25]. The intensity and correspondence of the (211), (300), and (202) diffraction peaks in the precursor powder and after nanoparticulation methods are observed, which highlights the production of pure HA nanoparticles. The slight change in peak width after ball mill and the peaks shift by XRD diffraction can be related to the fine-grained microstructure [32–34].

The strongest (211) peak at 31.9° corresponds to HA (P63/m), which belongs to the hexagonal symmetry (JCPDS 9–432). These results indicate that the dihydroxylation of HA and, as hydroxyl carbonate apatite, is beneficial for biomedical purposes owing to its similarity with bone apatite [27]. The peak of all carbonated calcium hydroxyapatite (CHA) at the (002) reflection was clearly broader. The characteristic peaks for β-TCP, which are located at the 2θ angles of 27.75, 31.65, 45.55, and 48.00° that normally do not appear in samples calcined at temperatures below a 1000 °C are evident in the methods for both samples, although less intensely present. The shape of the XRD peaks suggests a well crystallized particles, and the broadened nature implies that the grain sizes are on the nanometer scale [17]. The estimated average grain size is 32.08 nm for the sonochemical method and 51.15 nm for ball mill method using the Debye-Scherrer formula, which was consistent with that found in the TEM analysis.

Bovine HA presents 93% $Ca_{10}(PO_4)_6(OH)_2$ and 7% $Ca_3(PO_4)_2$ and

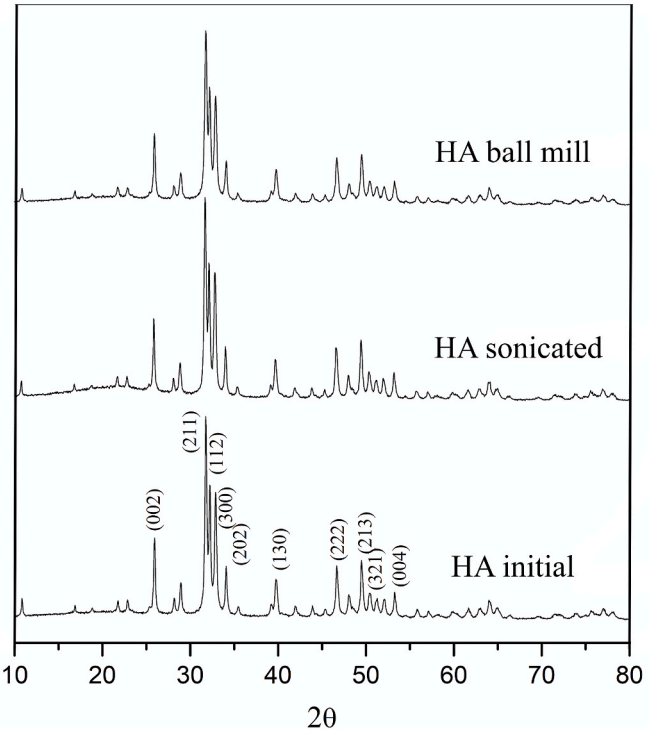

Fig. 3. The comparative XDR patterns of HA precursor and after the nanoparticulation methods. The ICDD involved card # 024–0033 for HA, # 009–0080 for CaHPO4, # 001–1160 for CaO and # 001–0941 for Ca3(PO4)2.

β-TCP as its crystalline phase composition. Its similarity to natural bone mineral has reported in previous literature [27], and in this study the HA crystallized in hexagonal space group P63/m. EDX allows for the qualitative and quantitative analysis of the inorganic elements present in a sample, and it confirmed the presence of Ca, P, and O (Fig. 4). The properties of hydroxyapatite are strongly dependent on its stoichiometry, the reactivity of its surface, and its biological behavior. Thus, the Ca/P molar ratio is one of the tools used to characterize the composition of different calcium phosphates. A Ca/P ratio of ≅ 1.92 fits with the acceptable range [35,36], so it appears to be a viable candidate for a

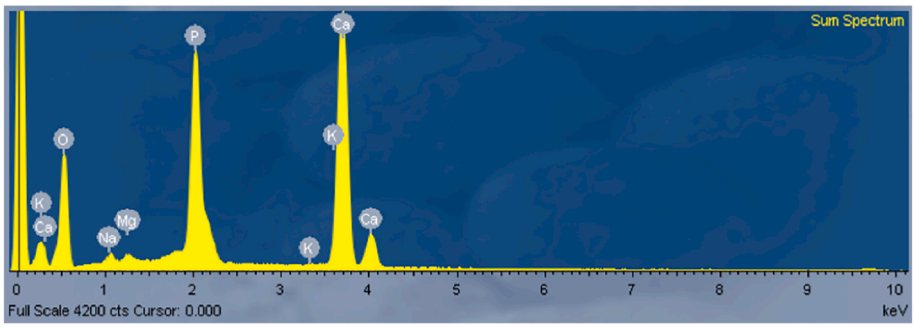

Fig. 4. Chemical characteristics for the three samples obtained by EDX.

bone substitute. HA that is extracted from mammalian sources contains trace elements that have optimum potential for enhancing the biological properties of natural HA, and these elements are not found in other sources [4]. Examples of these minor elements are Mg^{2+} and Na^{+}, which appear in our EDX samples, and are the most frequently found on spectrum.

The TEM images show the nanoparticle size and morphology of the HA samples. Figs. 5–7 shows TEM images of the initial, sonochemical, and ball milled samples, respectively. Different forms of HA crystallites—needles, flakes, spheres, rods, and plate-like—are indicated. The particle shape was not affected by the extraction method or source, and the same source of bone could produce different shapes [4]. In our experiments, the aggregation resulted in nanoflakes with an average size of ≅ 75 μm for the initial samples, ≅ 60 nm for sonicated, and ≅ 40 nm for ball milled samples (Figs. 8 and 9). Similar results were found by Ayatollahi et al. [15]. Samples that underwent the sonication technique showed difficulty in signaling diffraction. This could be justified by the presence of amorphous material around the nanoparticles. The sonochemical method is a wet-chemistry method, and the lattice parameters may have been negatively affected by water inclusion and/or atypical surroundings [37]. The deflocculant polymer in the aqueous medium encompassed the HA nanoparticle, which hindered the diffraction and formation of the crystalline plane (Fig. 6). For the ball milled samples in an alcohol medium, there was no such event, and the diffraction signal did not present any difficulty. There was competition between the amorphous phase and the crystalline phase; however, the sample diffracted (Fig. 7). Further studies are necessary to elucidate the interaction between the deflocculant polymer, HA nanoparticles, and the type of medium.

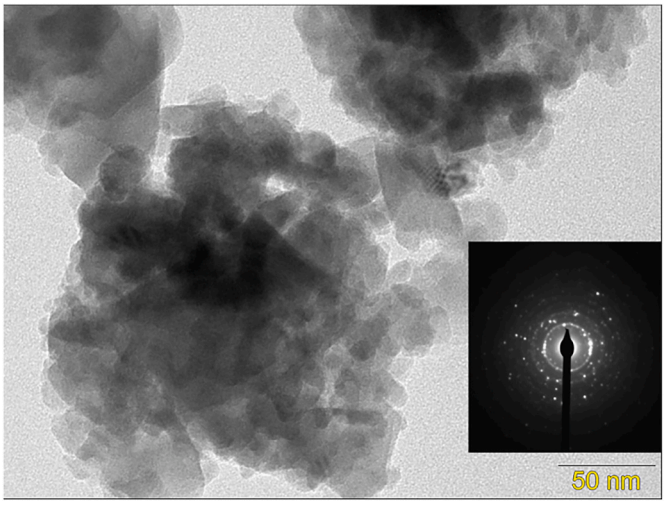

Fig. 5. TEM micrograph of the HA sonicated sample. In detail electron diffraction shows that this is a polycrystalline sample.

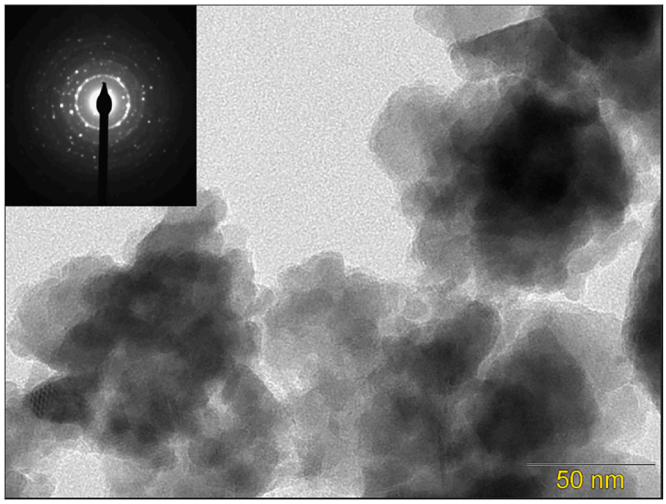

Fig. 6. TEM micrograph of the HA sonicated.

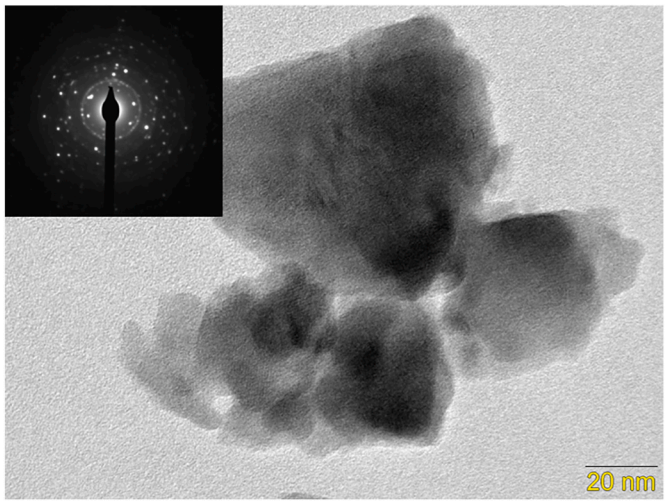

Fig. 7. TEM micrograph of the HA milled sample. In detail electron diffraction shows that this is a polycrystalline sample.

4. Conclusions

The present study demonstrated the viability of the nanoparticulation of bovine hydroxyapatite via the sonication and ball mill methods, combined with prior calcination. The samples maintained stoichiometry, morphology, and purity. Owing to the increasing demand for nano-HA in biomedical applications, it is important to elucidate

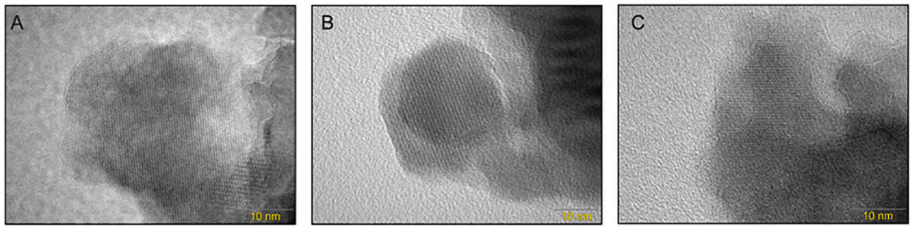

Fig. 8. TEM micrograph of initial (A), sonochemical (B) and ball mill (C) HA samples.

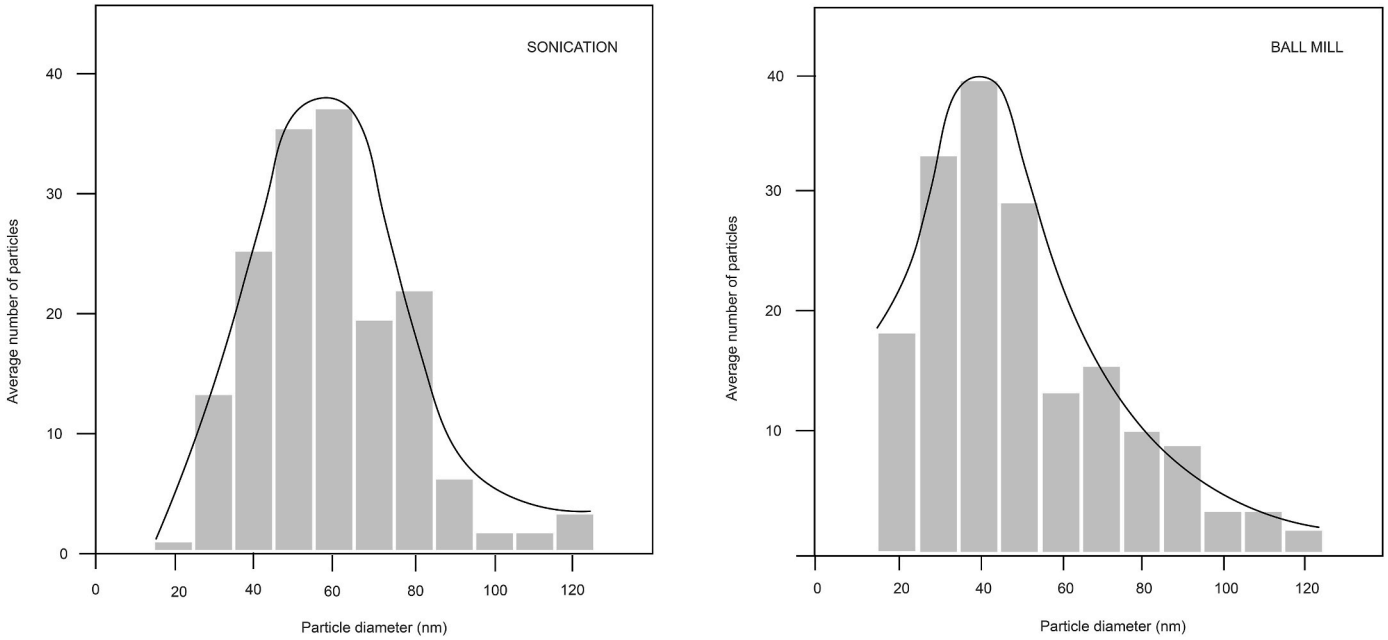

Fig. 9. TEM images allowed the construction of the distribution of number of particles histograms as a function of particle diameter for the samples sonicated and milled.

methods that are capable of obtaining phase purity, thermal stability, low cost, and from a sustainable source.

1 Bovine bone is a raw material and a suitable natural source for nano-hydroxyapatite.
2 The sonication (≅ 60 nm) and ball milling (≅ 40 nm) methods efficiently obtained particles on a nanometric scale, as indicated by TEM images and XRD analysis.
3 The XRD profile of both nanoparticulation methods has similar stoichiometric with initial HA indicating a high crystallinity and a single phase of HA.
4 The FTIR analysis showed a broad band at 1300–500 cm^{-1} and similar peaks, without the degradation of the HA bonds, regardless of the two forms of HA nanoparticles.
5 EDX demonstrated that the samples had the same chemical characteristics.

Funding

This work was supported by the São Paulo Research Foundation (FAPESP; grant number: 2018/23639-0) and the Coordination for the Improvement of Higher Education Personnel (CAPES, Finance Code 001).

CRediT authorship contribution statement

Brunna Mota Ferrairo: Conceptualization, Methodology, Formal analysis, Investigation, Writing – original draft, Writing – review & editing. **Victor Mosquim:** Methodology, Investigation, Writing – review & editing. **Lucas José de Azevedo-Silva:** Methodology, Investigation, Writing – review & editing. **Luara Aline Pires:** Methodology. **David Santos Souza Padovini:** Methodology, Writing – review & editing. **Aroldo Geraldo Magdalena:** All authors have read and agreed to the published version of the manuscript. **Carlos Alberto Fortulan:** Conceptualization, Writing – review & editing, Visualization. **Paulo Noronha Lisboa-Filho:** Writing – review & editing, Visualization, All authors have read and agreed to the published version of the manuscript. **José Henrique Rubo:** Writing – review & editing, Visualization, Funding acquisition. **Ana Flávia Sanches Borges:** Writing – review & editing, Visualization, Project administration.

Declaration of competing interest

The authors declare that they have no known competing financial interests or personal relationships that could have appeared to influence the work reported in this paper.

Data availability

No data was used for the research described in the article.

Acknowledgements

The authors are grateful for the support provided by São Paulo

Research Foundation (FAPESP), grant number: 2018/23639-0 and the Coordination for the Improvement of Higher Education Personnel (CAPES).

References

[1] L.L. Hench, Bioceramics - from concept to clinic, J. Am. Ceram. Soc. 74 (1991) 1487–1510.

[2] K. Schwarz, D.B. Milne, Growth-promoting effects of silicon in rats, Nature 239 (1972) 333–334.

[3] R. Jugdaohsingh, Silicon and bone health, J. Nutr. Health Aging 11 (2007) 99–110.

[4] E.M. Carlisle, Silicon: a possible factor in bone calcification, Science 167 (1970) 279–280.

[5] C.M. Botelho, R.A. Brooks, S.M. Best, M.A. Lopes, J.D. Santos, N. Rushton, et al., Human osteoblast response to silicon-substituted hydroxyapatite, J. Biomed. Mater. Res. 79 (2006) 723–730, https://doi.org/10.1002/jbm.a.30806.

[6] Q. Tang, R. Brooks, N. Rushton, S. Best, Production and characterization of HA and SiHA coatings, J. Mater. Sci. Mater. Med. 21 (2010) 173–181, https://doi.org/10.1007/s10856-009-3841-y.

[7] T. Gao, H.T. Aro, H. Ylänen, E. Vuorio, Silica-based bioactive glasses modulate expression of bone morphogenetic protein-2 mrna in saos-2 osteoblasts in vitro, Biomaterials 22 (2001) 1475–1483.

[8] I.D. Xynos, A.J. Edgar, L.D. Buttery, L.L. Hench, J.M. Polak, Gene-expression profiling of human osteoblasts following treatment with the ionic products of bioglass 45s5 dissolution, J. Biomed. Mater. Res. 55 (2001) 151–157.

[9] N. Patel, S.M. Best, W. Bonfield, I.R. Gibson, K.A. Hing, E. Damien, P.A. Revell, A comparative study on the in vivo behavior of hydroxyapatite and silicon substituted hydroxyapatite granules, J. Mater. Sci. Mater. Med. 13 (2002) 1199–1206, https://doi.org/10.1023/a:1021114710076.

[10] J.D. de Bruijn, Y.P. Bovell, J.E. Davies, C.A. van Blitterswijk, Osteoclastic resorption of calcium phosphates is potentiated in postosteogenic culture conditions, J. Biomed. Mater. Res. 28 (1994) 105–112, https://doi.org/10.1002/jbm.820280114.

[11] E.M. Carlisle, Silicon: a requirement in bone formation independent of vitamin D1, Calcif. Tissue Int. 33 (1981) 27–34, https://doi.org/10.1007/BF02409409.

[12] M. Sadat-Shojai, M.T. Khorasani, E. Dinpanah-Khoshdargi, A. Jamshidi, Synthesis methods for nanosized hydroxyapatite with diverse structures, Acta Biomater. 9 (2013) 7591–7621.

[13] N.A.S. Mohd Pu'ad, P. Koshy, H.Z. Abdullah, M.I. Idris, T.C. Lee, Syntheses of hydroxyapatite from natural sources, Heliyon 5 (2019), e01588.

[14] I.R. Gibson, S.M. Best, W. Bonfield, Chemical characterization of silicon-substituted hydroxyapatite, J. Biomed. Mater. Res. 44 (1999) 422–428, https://doi.org/10.1002/(sici)1097-4636(19990315)44:4<422::aid-jbm8>3.0.co;2-#.

[15] M.R. Ayatollahi, M.Y. Yahya, H.A. Shirazi, S.A. Hassan, Mechanical and tribological properties of hydroxyapatite nanoparticles extracted from natural bovine bone and the bone cement developed by nano-sized bovine hydroxyapatite filler, Ceram. Int. 42 (2015) 10818–10827.

[16] M.J. Coathup, S. Samizadeh, Y.S. Fang, T. Buckland, K.A. Hing, G.W. Blunn, The osteoinductivity of silicate-substituted calcium phosphate, the journal of bone and joint surgery, American volume 93A (2011) 2219–2226, https://doi.org/10.2106/Jbjs.J.01623.

[17] M. Wiens, M. Bausen, F. Natalio, T. Link, U. Schlossmacher, W.E. Muller, The role of the silicatein-alpha interactor silintaphin-1 in biomimetic biomineralization, Biomaterials 30 (2009) 1648–1656, https://doi.org/10.1016/j.biomaterials.2008.12.021.

[18] A. Rai, C.C. Perry, Facile Fabrication of uniform silica films with tunable physical properties using silicatein protein from sponges, Langmuir 26 (2010) 4152–4159, https://doi.org/10.1021/La903366a.

[19] C.M. Botelho, M.A. Lopes, I.R. Gibson, S.M. Best, J.D. Santos, Structural analysis of Si-substituted hydroxyapatite: zeta potential and X-ray photoelectron spectroscopy, J. Mater. Sci. Mater. Med. 13 (2002) 1123–1127.

[20] P. Kalia, R.A. Brooks, S.D. Kinrade, D.J. Morgan, A.P. Brown, N. Rushton, et al., Adsorption of amorphous silica nanoparticles onto hydroxyapatite surfaces differentially alters surfaces properties and adhesion of human osteoblast cells, PLoS One 11 (2016), e0144780, https://doi.org/10.1371/journal.pone.0144780.

[21] M. Borden, M. Attawia, Y. Khan, C.T. Laurencin, Tissue engineered microsphere-based matrices for bone repair: design and evaluation, Biomaterials 23 (2002) 551–559.

[22] M.M. Pereira, L.L. Hench, Mechanisms of hydroxyapatite formation on porous gel-silica substrates, J. Sol. Gel Sci. Technol. 7 (1996) 59–68.

[23] L.A. Pires, L.J. de Azevedo Silva, B.M. Ferrairo, R. Erbereli, J.F.P. Lovo, O. Ponce Gomes, J.H. Rubo, P.N. Lisboa-Filho, J.A. Griggs, C.A. Fortulan, A.F.S. Borges, Effects of ZnO/TiO2 nanoparticle and TiO2 nanotube additions to dense polycrystalline hydroxyapatite bioceramic from bovine bones, Dent. Mater. 36 (2020) e38–e46, https://doi.org/10.1016/j.dental.2019.11.006.

[24] R.R. Srinivasa, A.K. Saad, Shear-thickening response of fumed silica suspensions under steady and oscillatory shear, J. Colloid Interface Sci. 185 (1997) 57–67.

[25] R. Erbereli, Avaliação da qualidade óssea de bovinos [master thesis], São Carlos: Universidade de São Paulo, Bioengenharia, 2017, https://doi.org/10.11606/D.82.2018.tde-20082018-121530.

[26] K.A. Hing, P.A. Revell, N. Smith, T. Buckland, Effect of silicon level on rate, quality and progression of bone healing within silicate-substituted porous hydroxyapatite scaffolds, Biomaterials 27 (2006) 5014–5026.

[27] E.E. Sych, N.D. Pinchuk, V.P. Klimenko, I.V. Uvarova, A.B. Togstonog, T.V. Tomila, Synthesis and properties of Si-modified biogenic hydroxyapatite ceramics, Powder Metall. Met Ceram. 54 (2015) 67–73, https://doi.org/10.1007/s11106-015-9681-z.

[28] R. Tolouei, C.Y. Tan, S. Ramesh, I. Sopyan, W.D. Teng, Effect of nano silica on the sinterability of hydroxyapatite dense bodies, Adv. Mater. Res. (2011) 264–265, 1832-1838, https://doi.org/10.4028/www.scientific.net/AMR.264-265.1832.

[29] I.G. Turner, Ceramics and glasses, in: R. Narayanan (Ed.), Biomedical Materials, Springer, New York, NY, USA, 2009, pp. 3–39.

[30] C.P. Whitby, M. Krebsz, S.J. Booty, Understanding the role of hydrogen bonding in the aggregation of fumed silica particles in triglyceride solvents, J. Colloid Interface Sci. 527 (2018) 1–9.

[31] P. Bowen, C. Carry, From powders to sintered pieces: forming, transformations and sintering of nanostructured ceramic oxides, Powder Technol. 128 (2002) 248–255.

[32] F. Erdemir, Study on particle size and X-ray peak area ratios in high energy ball milling and optimization of the milling parameters using response surface method, Measurement 112 (2017) 53–60, https://doi.org/10.1016/j.measurement.2017.08.02.

[33] E.D. Yalçın, A. Çanakçı, F. Erdemir, H. Çuvalci, A.H. Karabacak, Enhancement of wear and corrosion resistance of ZA27/nanographene composites produced by powder metallurgy, Arabian J. Sci. Eng. 44 (2019) 1437–1445, https://doi.org/10.1007/s13369-018-3582-7.

[34] O. Güler, F. Erdemir, M. Çeleibi, H. Çuvalci, A. Çanakçi, Effect of nano alumina content on corrosion behavior and microstructure of Za27/graphite/alumina hybrid nanocomposites, Results Phys. 15 (2019), 102700, https://doi.org/10.1016/j.rinp.2019.102700.

[35] R. Chaim, M. Levin, A. Shlayer, C. Estournès, Sintering and densification of nanocrystalline ceramic oxide powders: a review, Adv. Appl. Ceram. 107 (2008) 159–169.

[36] V. Mosquim, B.M. Ferrairo, M. Vertuan, A.G. Magdalena, C.A. Fortulan, P. N. Lisboa-Filho, P.F. Cesar, E.A. Bonfante, H.M. Honório, A.F. Sanches Borges, Structural, chemical and optical characterizations of an experimental SiO2-Y-TZP ceramic produced by the uniaxial/isostatic pressing technique, J. Mech. Behav. Biomed. Mater. 106 (2020), 103749, https://doi.org/10.1016/j.jmbbm.2020.103749.

[37] M. Vallet-Regí, C.V. Ragel, A.J. Salinas, Glasses with medical applications, Eur. J. Inorg. Chem. (2003) 1029–1042.